Climate-linked escalation of societally disastrous wildfires

Calum X. Cunningham[1]*, John T. Abatzoglou[2], Crystal A. Kolden[2], Grant J. Williamson[1], Markus Steuer[3], David M. J. S. Bowman[1]

[1] Fire Centre, School of Natural Sciences, University of Tasmania, Hobart, Australia

[2] Department of Management of Complex Systems, University of California, Merced, Merced, CA, USA

[3] Geo Risks, Munich Re, Munich, Germany

* corresponding author: calum.cunningham@utas.edu.au

Abstract

Climate change is forcing societies to contend with increasingly fire-prone ecosystems. Yet, despite evidence of more extreme fire seasons, evidence is lacking globally for trends in wildfires with socially and economically disastrous effects. Using a systematic dataset, we analyse the distribution, trends, and climatic conditions connected with the most lethal and costly wildfire disasters from 1980-2023. Disastrous wildfires occurred globally but were disproportionately concentrated in the Mediterranean and Temperate Conifer Forest biomes, and in populated regions that experience intense fire. The frequency of disastrous wildfires increased sharply from 2015, with 43% of the 200 most damaging events occurring in the last 10 years. Major disasters coincided with extreme climatic conditions, and such conditions significantly increased from 1980-2023, highlighting the urgent need to adapt to a more fire-prone world.

Introduction

Wildfire is a fundamental Earth system process that influences ecosystem dynamics, biogeochemical cycling, and socio-ecological systems (*1, 2*). Humans and our congeners have co-existed with fire for at least 400,000 years (*1*) and every continent except Antarctica has fire-adapted biomes (*3*). Despite this long coexistence with fire, anthropogenic climate change is now rapidly altering fire conditions around the world, presenting major challenges for inhabiting flammable landscapes (*4, 5*).

Climate change has already caused fire weather to depart from its historical variability across ~20% of burnable land area globally (*6*). This change is largely driven by rising temperatures and increasing vapor pressure deficit (*7, 8*), leading to drier fuels (*9*), more extreme fire weather (*10*), and prolonged fire seasons (*11*). In some areas, these changes are compounded by high fuel loads stemming from a constellation of factors including long-term fire suppression, curtailment of Indigenous burning, spread of exotic species, and changes in land use and management (*12*). Consequently, fire activity is increasing in some regions, including the forests of western Canada (*13*), Australia (*14*), western United States (*15*), and high latitudes (*16, 17*), contributing to a doubling of energetically extreme fires over the last 10 years (*17*). Importantly, this change has occurred despite the global decline in area burned over the last two decades (mostly driven by fire regime changes in arid grasslands and tropical savannas (*2, 18*)). The societal effects of changing fire regimes are further compounded by human population growth and an expanding wildland-urban interface (*19-22*).

Scientific papers and the media are pervaded by the notion that societally disastrous wildfires – those that cause major economic losses or deaths – are becoming increasingly common (*23*). Yet, prior analyses do not support this view, with analysis of a long-term global disaster database, Emergency Events Database (EM-DAT), reporting no temporal trends in the direct economic losses (1987-2014) and fatalities (1977-2014) caused by wildfires (*23*). The period since that analysis, however, has been punctuated by major fire disasters with disturbing regularity: in 2016, the Fort McMurray Fire caused US$4b damage, the costliest in Canadian history (*24*). In 2017, several major fires in California caused a combined ~US$15b in damages, the largest losses at the time (25). In 2018, the costliest fire in history, the Camp Fire (Paradise, California; US$16.5b (26)), killed 85 people, only to be eclipsed in 2023 by the Lahaina Fire (Hawaii) that caused 101 fatalities, the most lethal in modern US history.

Major events have also occurred in Portugal (2017), eastern Australia (2019/2020), Algeria (2021), Greece (2018, 2021, and 2023), and Chile (2017, 2023, and 2024), with the most recent major event in Chile causing 135 fatalities (*27*). Thus, although fire conditions and regimes are clearly changing (*2, 13-18, 28*) and major events are seemingly mounting, there remains no systematic evidence of global changes in the frequency or magnitude of societally disastrous wildfires (23).

Here, we analyse systematic records of wildfire disasters from 1980-2023 to identify geographic and temporal trends in wildfire disasters. To do this, we harmonised two systematic global disaster databases that report economic losses and fatalities associated with wildfires. NatCatSERVICE (*29*) is one of the world's most comprehensive (but private) global disaster datasets compiled by Munich Re, a leading global reinsurance company. It follows a standardised methodology, with the dataset suitable for trend analysis from 1980 onwards (*29*). To complement NatCatSERVICE, we also incorporated the publicly available EM-DAT, compiled by the Centre for Research on the Epidemiology of Disasters (*30*). Using these data, we identified major disasters, defined here as events causing 10 or more fatalities (matching EM-DAT's criteria) and the 200 largest economic losses as a percentage of a country's gross domestic product (GDP) at the time, providing an economic measure that is comparable across economies. Using this novel dataset, we (1) quantify changes in the frequency and magnitude of major wildfire disasters, (2) characterise and model the geographic distribution of major wildfire disasters, and (3) identify the climatic conditions associated with wildfire disasters and evaluate whether such conditions have become more common due to climate change.

Upward trend of disastrous wildfires

Across multiple metrics, there was strong evidence that wildfire disasters are increasingly burdening societies around the world. Major economic losses caused by wildfire events increased by ~4.4-fold from 1980-2023 ($p < 0.0001$, Fig 1a). Of the 200 most damaging events, 43% occurred in the last 10 years (Fig 1a). There was no evidence that the increasing trend is confined to a particular region (Table S2; Fig S5).

Damage as a percentage of global GDP peaked in 2018 at 5.1 times higher than the 44-year average, totalling US$28.3 billion and 0.03% of global GDP (Fig 1d-e). The large increase in absolute damage costs was strongly driven by North America (Fig 1d) where prices are comparatively high. Total damage costs were strongly influenced by singular events (Fig S6), primarily in the western USA, typifying the skewed distributions characteristic of natural disasters (*31*). There have been 43 billion-dollar events (2022 USD) since 1980, of which 51% occurred in the last 10 years (Fig 1c). Although this trend was similarly dominated by North America, billion-dollar events also occurred in Asia, Oceania (southern Australia and Indonesia), and Europe in the last decade (Fig 1c).

The frequency of major fatality events causing 10 or more deaths ($n = 85$ events) increased by 3.1-fold from 1980-2023 ($p = 0.004$; Fig 1b), during which the human population increased by 1.8-fold. This increase in major fatality events highlights the most urgent part of the disaster adaption pathway to address, wherein prioritizing improved communication and evacuation planning can facilitate protecting lives (*32*). Such preparedness activities focused on life safety, however, are also critical for saving property because firefighting resources can be redirected from search and rescue to structure protection (*33*).

It is important to note that the effects analysed here represent only an index of the overall societal costs of wildfire because they do not include indirect losses or indirect fatalities. For example, the tens of thousands of fires that burned in Indonesia in 2015 were estimated to cause $1.2b in direct damage, but the World Bank estimated a much larger overall cost to the Indonesian economy of $19.9b (adjusted to 2022 USD; *34*). Similarly, disaster datasets also likely underestimate wildfire fatalities, and do not delineate civilian from firefighter (i.e., line of duty) fatalities, which likely have different patterns. As noted by Doerr and Santín (*23*), wildfire causes fewer direct mortalities than earthquakes, floods, and storms. Nevertheless, there is likely a much larger underreporting problem for wildfire because the indirect effects of smoke often influence much broader regions and usually go unquantified (*35*). For instance, EM-DAT reported 19 direct deaths from the 2015 Indonesian fires, but the resulting smog that blanketed much of southeast Asia was implicated in as many as ~100,000 additional premature deaths from respiratory problems (*36*) that are not present in such disaster databases.

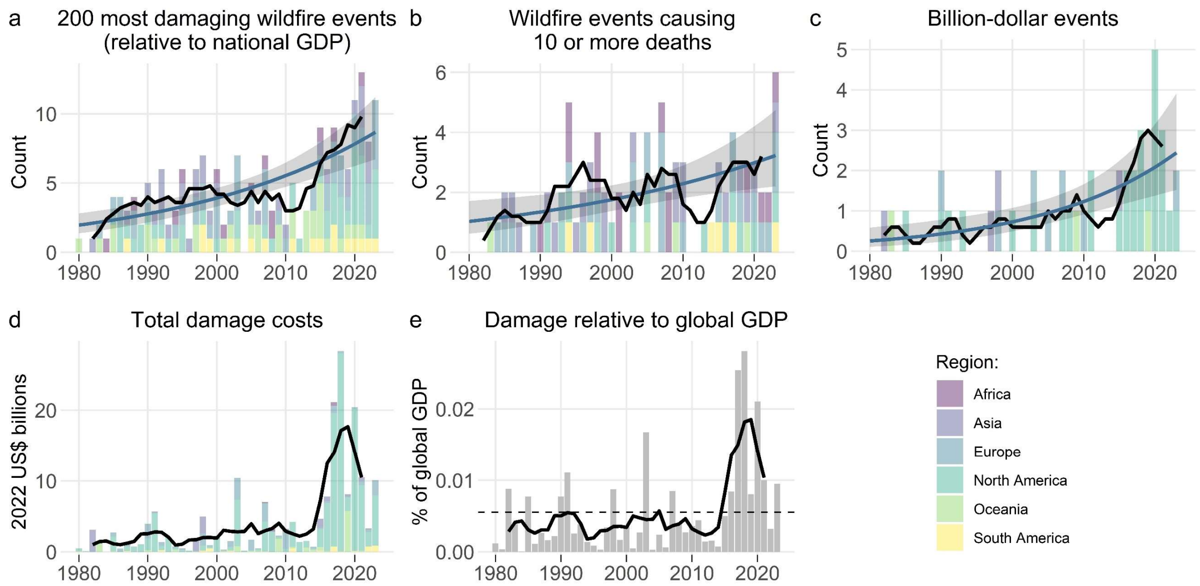

Figure 1. Increasing frequency and severity of wildfire disasters. *In each panel, black lines show the 5-year rolling average.* ***(a)*** *Temporal distribution of the 200 most damaging wildfire events, measured as a percentage of a country's contemporaneous GDP. The blue line shows the fit of a GLM (± 95% CI).* ***(b)*** *Temporal trends in wildfire events that led to large losses of life, defined by EM-DAT as at least 10 fatalities, with the blue line showing the fit of a GLM (± 95% CI).* ***(c)*** *The annual frequency of billion-dollar events (2022 USD).* ***(d)*** *Total damage costs of wildfire disasters, calculated from all events (not just the top 200).* ***(e)*** *Total damage costs expressed as a percentage of global GDP, with the dashed line showing the 44-year mean. See Fig S5 for separate regional graphs of panel a, and Table S3 for model coefficients for a-c.*

Pyrogeography of major wildfire disasters

Major wildfire disasters occurred globally, but they had distinct pyrogeographic patterns and biome specificity (Fig 2 and Fig 3). Disasters were heavily concentrated in the Mediterranean Forest/Woodland/Scrub Biome (Europe, southern South America, western USA, South Africa, and southern Australia) and the Temperate Conifer Forest Biome (mostly western North America), where disasters occurred 12.1 and 4.1 times more than expected based on the areas of those biomes, respectively (Fig 2). Relative to the population sizes of the biomes, the Temperate Conifer Forest Biome, Mediterranean Biome, and Boreal Forest Biome experienced 7.6, 6.8 and 8.2 times more disasters than expected based on their population sizes, respectively (Fig 2).

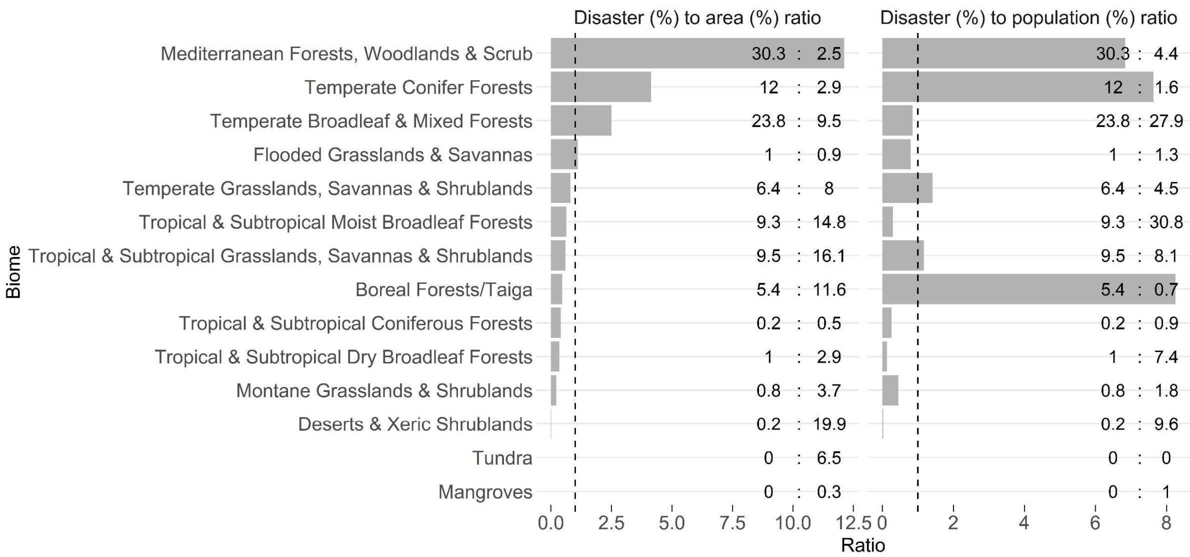

Figure 2. Patterns in the distribution of major wildfire disasters relative to the areas and population sizes of the biomes. *The ratio was calculated by dividing the percentage of all major disasters occurring in a biome (left numbers in each sub-plot) by the percentage of the global area or global population in each biome (right numbers in each sub-plot). Values >1 (dashed vertical line) indicate more disasters than expected based on the biome's area or population size, and values less than one indicate lower than expected disaster rate. Biome population sizes in each year were based on the nearest available year (1990, 1995, 2000, 2005, 2015, 2020) using the Gridded Population of the World dataset, v3 and v4 (37).*

Building on these descriptive patterns (Fig 2), we constructed a disaster distribution model, analogous to a species distribution or habitat suitability model, to identify environmental relationships distinguishing disaster locations from background locations. The best-performing model contained effects of biome, geographic region, summed nighttime fire radiative power (ΣFRP_{night}), and human population density (out-of-sample $AUC_{ROC} = 0.91$; Table S5). Disasters were most likely to occur in Oceania (particularly Australia) and least likely in Africa, despite most fire occurring in Africa (Fig 3b; Fig S3). Major disasters were concentrated in areas where relatively intense fires co-occur with areas populated by humans (Fig 3d), rather than where the most fire occurs (i.e., tropical savannahs of Africa and northern Australia; Fig S3). The best-supported model, which contained ΣFRP_{night}, performed substantially better than models containing other metrics of fire ($\Sigma FRP_{day/night}$, day/night hotspot density, and night hotspot density; Table S5). This indicates that areas where intense fires burn overnight, as opposed to more benign human-driven day-only fires, typify locations where major disasters are most likely to occur.

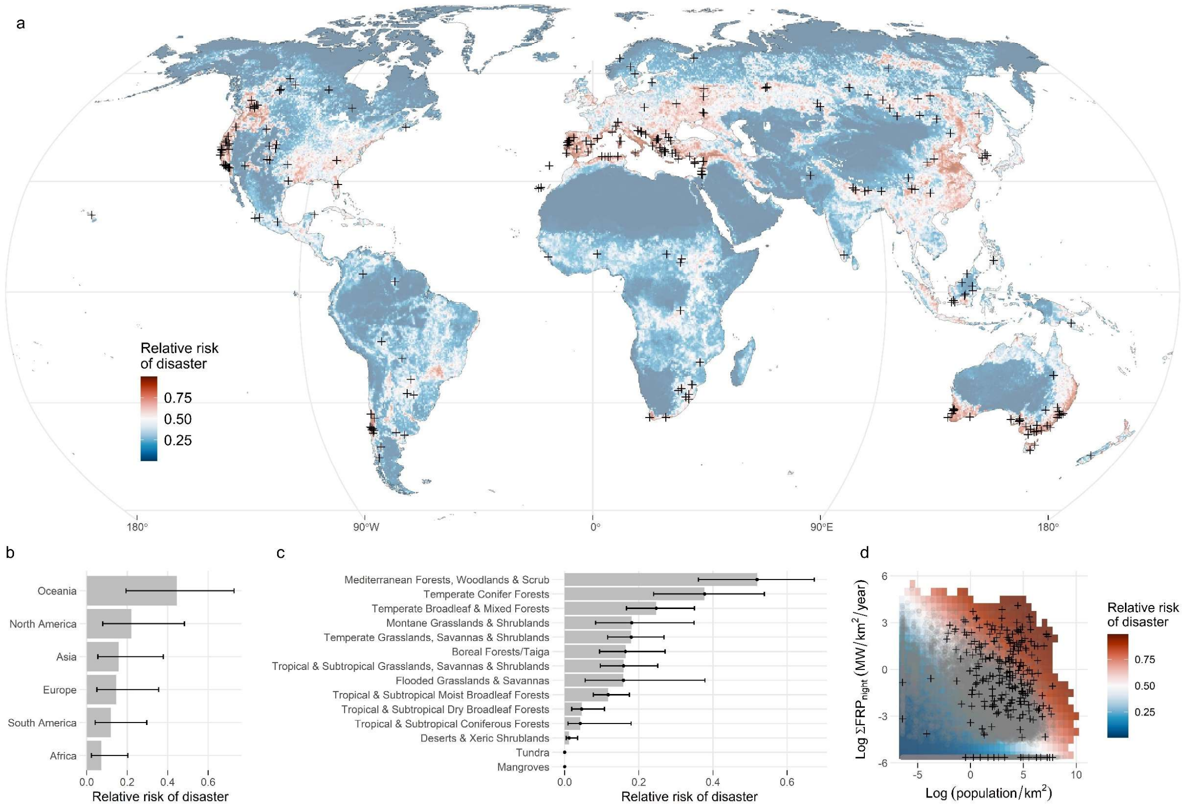

***Figure 3. The distribution of major wildfire disasters**. (**a**) The locations of 242 major wildfire disasters, defined as the 200 most economically damaging wildfires (relative to contemporaneous national GDP) and events that caused 10 or more fatalities (n = 85), with 43 jointly comprising major economic and major fatality events. Crosses show disaster locations overlayed on relative risk (or probability) predicted by a generalised additive model of disaster locations and background locations. (**b-d**) Effects plots show the model fit (± standard error), while holding other variables constant. In d, black crosses show disasters and grey dots show background points. See Table S4 for a breakdown of the number of events in the biomes of each region and Fig S3 for a map of the biomes.*

The climate signature of wildfire disasters

Major wildfire disasters typically coincided with extreme fire weather and drought (Fig 4a-b), and such conditions increased in frequency and severity from 1979-2023 (Fig 4c and Fig 5). Extremes for fire weather index (FWI_{max}), vapor pressure deficit (VPD_{max}), and drought severity ($PDSI_{max}$; inverted Palmer Drought Severity Index) were each significantly higher during disasters compared to the same period in non-disaster years (Fig 4b). FWI_{max} exhibited the largest difference, on average, at an estimated 1.61 standard deviations above the average FWI_{max} for the Julian days of each disaster (one-sample t-test; $p < 0.001$, $t = 19.7$; Fig 4b). Fire disasters often coincided with concurrent high fire weather, high vapor pressure deficit, and high long-term drought stress (Fig 4b). For example, 83% of disasters occurred while FWI_{max} and VPD_{max} were both higher than the average time-matched extreme, and 77% of disasters occurred while both drought stress and fire weather were high (Fig 4b). Further, 50% of disasters had FWI_{max} exceeding the 99.8th percentile of FWI (calculated over all days).

The frequency and severity of such “fire disaster weather” increased substantially during the period 1979-2023. For example, the annual extreme value for the Julian days of each disaster showed a sustained migration from the lower-risk quadrant (bottom left) to the higher-risk quadrant (top right) of the bivariate relationships (Fig 4c). FWI_{max}, VPD_{max}, and $PDSI_{max}$ were each significantly higher in the period 2001-2023 compared to 1979-2000 ($p < 0.001$ for all two-sample t-tests; Fig 4c). Similarly, the proportion of days (FWI, VPD) and months (PDSI) exceeding the local 99.8th percentile (calculated over all days, corresponding to median FWI_{max} during the disasters) increased by 2.4-fold for FWI, 3.9-fold for VPD, and 7.3-fold for PDSI from 1979-2023 (Fig 5). These dual findings – that major wildfire disasters are tightly linked with extreme conditions (Fig 4b), and that climate change has substantially increased the frequency and severity of such “disaster weather” (Fig 4c, Fig 5) – suggest a considerable role of climate change in driving the increase of major wildfire disasters.

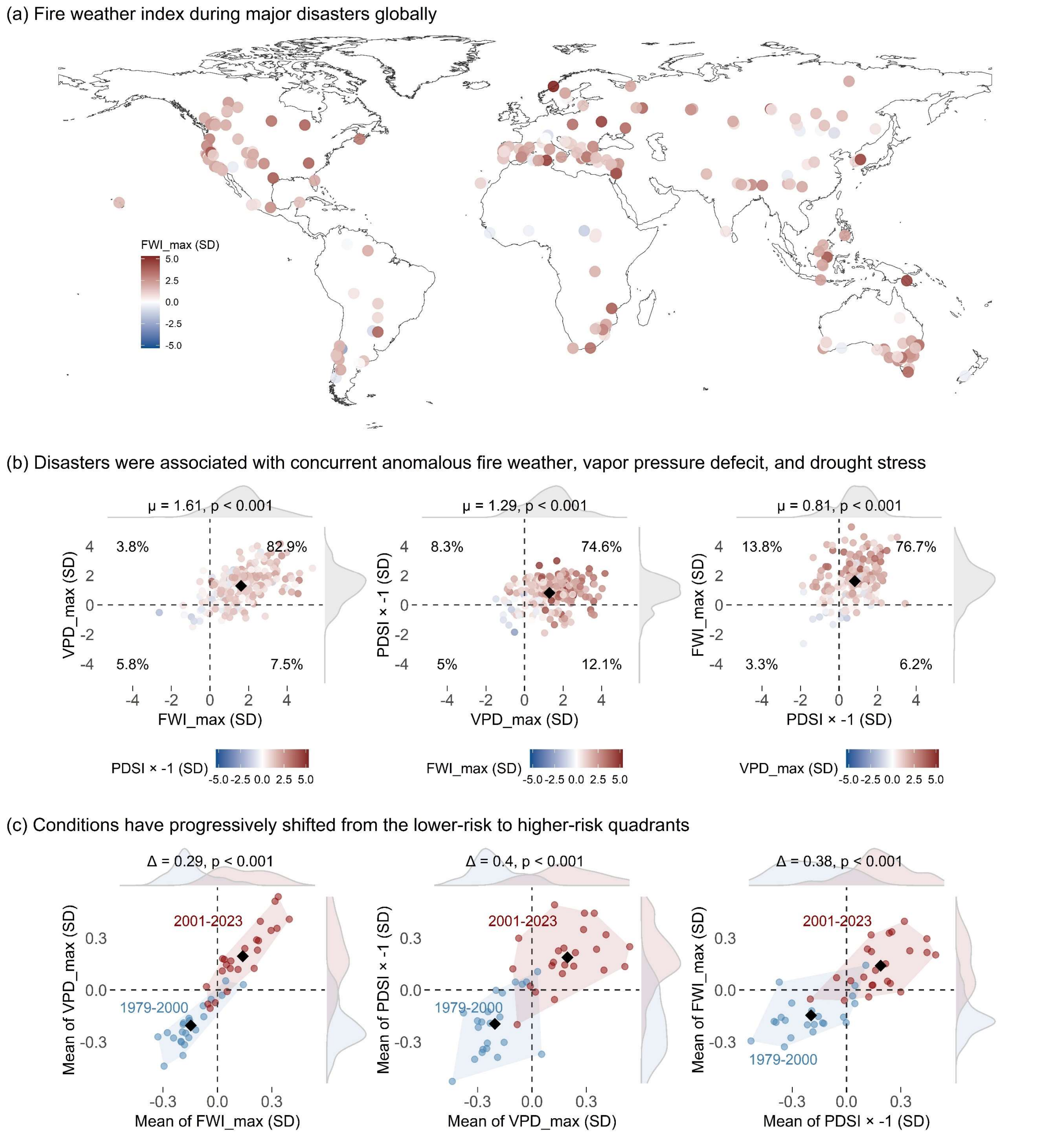

Figure 4. Associations between major wildfire disasters and climatological conditions. *For each disaster location, values were calculated by identifying the maximum value during the Julian days of each disaster in each year from 1979-2023. Values were z-score standardised by subtracting the mean and dividing by the standard deviation for the same Julian day ranges (for each location separately).* ***(a)*** *Globally, FWI_{max} was almost always higher than the average extreme for the Julian days of the disasters. Points show FWI_{max} of each fire disaster.* ***(b)*** *Disasters typically coincided with conditions that had high concurrent FWI_{max}, VPD_{max}, and PDSI [× -1], relative to maximum values in the time-matched periods of non-disaster years. Points show the anomaly during the disasters. Black diamonds show the means, and p-values indicate the significance of a one-sample t-test of whether the disaster anomalies differed from the mean value (i.e., zero).* ***(c)*** *Extreme days have become more anomalous from 1979-2023. Points show the mean extreme corresponding the Julian day period of each disaster (i.e., mean of 240 extreme values each year). Δ denotes the difference between mean values in 1979-2000 compared to 2001-2023, and p indicates the significance of two-sample t-tests.*

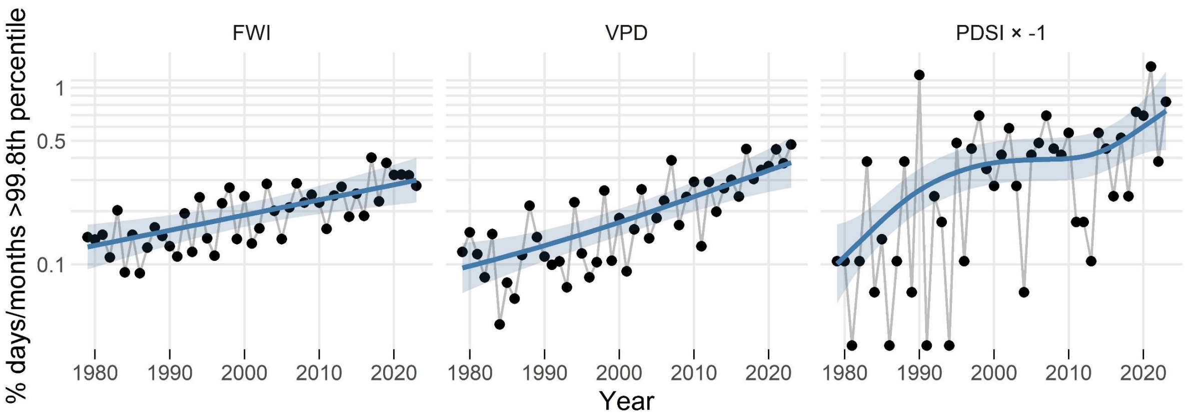

Figure 5. Increasing frequency of extreme fire weather index, vapor pressure deficit, and Palmer drought stress index. *Points show the percentage of days (FWI and VPD) and months (PDSI) in each year at the disaster locations that exceeded the 99.8th percentile value, calculated over all days from 1979-2023 (which corresponds to median FWI_{max} during the disasters). The blue line shows the fit of a generalized additive model.*

Discussion

Our analysis of trends in wildfire disasters revealed a global-scale fire disaster crisis. Some regions are more prone to wildfire disasters because of their biogeography, most notably, the Mediterranean forest/woodland/scrub, temperate conifer forest, and boreal forest biomes. People living in those biomes experienced the highest per capita rates of disaster. This pattern aligns with other work showing that these three biomes are disproportionately exposed to energetically extreme wildfires, which have more than doubled in frequency over the last two decades globally (*17, 38*).

Disasters coincided with conditions unusually conducive to extreme fire, and climate change is making such "disaster weather" more common (Fig 4c & 5). This finding fits with growing evidence that climate change is increasing fire weather (*10, 11, 39*), the number of days suitable for extreme daily fire growth (*40*), burned area in forests (*13-17*), coincidence of downslope winds and drought conditions (*41, 42*), and fire at night during which firefighters have typically been afforded respite (*43, 44*). Indeed, other work shows that climate change has increased the probability of extreme fire weather by 40% in regions of California that experienced extreme fire disasters in 2017 and 2018 (*45*). While there was a strong climate signal in our analysis of the disaster data, other processes including increasing exposure caused by the expanding wildland-urban interface and agricultural land abandonment are implicated in the trend (*20-22, 46, 47*). Contextual differences necessitate finer-scale studies to reveal local-scale causes and illuminate opportunities for adaptation, such as building standards, fuel loads, forestry practices, and the role of fire behaviour in different vegetation types (*48, 49*). Radeloff et al. (*20*), for example, show that increases to burned area and the WUI have had similar-sized influences on the rising risk to houses in the USA, and this risk is most pronounced near grasslands and shrublands rather than forests.

The exposure of regional communities in affluent countries is having significant global financial impacts. For instance, the "Camp Fire" which destroyed 18,804 structures in the regional community of Paradise, California, was the largest insured event of all natural perils in 2018 (*50*). Once considered a secondary peril of minor importance by global reinsurance companies (i.e., insurers of insurers), wildfire is now a serious concern and is even leading to the failure of significant financial markets. Major home insurers in California, for example, are refusing to renew insurance policies or issue new ones because of rising financial exposure to catastrophes (*51*) and because major losses have wiped out more than twice the aggregate profits of the previous two decades (*52*). While events in lower-income countries often receive less attention because they cause smaller absolute losses, our approach of relativising losses as a percentage of a country's GDP means that trends in lower-income countries are importantly captured in the global trends. However, even despite normalising losses by GDP, it is possible that some bias remains, given probable differences among regions in ease of communication and coverage of disasters (*53, 54*). The map of disaster risk highlights some locations that may suffer non-negligible reporting biases, such as eastern China where modelled disaster risk is relatively high despite only a modest number of disasters having been reported (Fig 3a).

Ballooning expenditure on fire suppression has not prevented the rising occurrence of wildfire disasters (*55*). While there is a lack of global data on fire suppression expenditure (*56*), inflation-adjusted US federal expenditure on fire suppression increased by ~3.6-fold from 1985-2022, peaking at $4.4B USD in 2021 (Fig S7). This expenditure is limiting (or masking) the fire crisis, but not offsetting it. Critical counterfactuals to consider are what would the trends have been in the absence of such investment or if suppression funds had been proactively spent on mitigation? And how will trends change as climate change outpaces and overwhelms current firefighting capacity, such as occurred in Canada in 2023 (*57*)? Destruction of entire towns or suburbs in recent disasters, including Santa Olga, Chile (2017) (*48*), Paradise, California, USA (2018) (*58*), and Lytton, British Columbia, Canada (2021) (*13*), provide glimpses into those counterfactuals. Investment in suppression capacity is essential, but overuse of fire suppression in the absence of proactive fire mitigation has produced the 'fire paradox' (*59*) by encouraging development in fire-prone settings and making fires burn more intensely when they do burn (*60*). This is akin to the 'safe development paradox' in flood and hurricane protection, whereby making dangerous areas safe for human habitation in the short-run increases potential for catastrophe in the long-run (*4, 61*).

Many of the costliest disasters (e.g., Camp Fire, Lahaina Fire) began as wildfires but transitioned into urban conflagrations via building-to-building transmission. Calkin et al. (*62*) frame these fire disasters as a problem of urban environments encroaching on wildlands, leading to urban conflagrations that propagate via building-to-building transmission. This feature highlights the importance of strategies that reduce transmission, including retrofitting existing structures, using stringent fire-sensitive design and materials in new builds, establishing defendable space, and removing nearby fuel in the home ignition zone (*58, 63-65*). In the US, there have also been substantial calls for managed retreat from living in the WUI as an adaptive response to increasing wildfire disasters, but this neglects both the long history of Indigenous peoples co-existing with fire in such regions (*66*) and the potential for exacerbating housing shortages that already negatively impact socially vulnerable populations in high-cost regions like California (*53, 67*). Many of the wildfire disasters in our analysis occurred in areas that have been urbanised for centuries to millennia (e.g., Rhodes, Greece; Cape Town, South Africa), suggesting that wildfire adaptation is a more viable strategy than avoidance.

Fire is an inevitable natural process essential for the health of fire-adapted ecosystems, and society must adapt to sustainably inhabit landscapes that are becoming increasingly fire prone (*4, 23*). This requires managing ecosystems so that fire does not become uncontrollably intense. The path forward must draw on and welcome the ancient wisdom and skills of Indigenous cultural burning (*68*). For example, Australian Indigenous people skilfully cultivated low-intensity fire regimes for millennia, but European invasion disrupted these regimes, leading to a thickening of shrubby understory in southeast Australian forests (*69*). Management of wildland fuels through targeted prescribed burning intends to reduce the intensity of fire; for example, low-intensity fire in California was shown to reduce risk of subsequent high-intensity wildfires by 64% for at least 6 years after fire (*70*). But reintroducing fire to vegetation with high fuel loads is not always straightforward. In such situations, approaches like mechanical thinning followed by intentional fire provide a potential pathway to reinstating low-intensity fire regimes (*71-74*). Mitigation pathways must also address strategies to reduce fatalities by increasing evacuation effectiveness and developing plans that account for socially vulnerable populations, who are the most likely be killed in wildfires (*53*). Like all fuel management strategies, best approaches will depend heavily on ecological context (*4*). To quell the emerging fire disaster crisis and adapt to an increasingly fire-prone climate, we must urgently test, embrace, deploy, and incentivize the diversity of available mitigation options at scales ranging from the wildland to the home ignition zone (*5*).

References

1. D. M. J. S. Bowman *et al.*, Fire in the Earth System. *Science* **324**, 481-484 (2009).
2. N. Andela *et al.*, A human-driven decline in global burned area. *Science* **356**, 1356-1362 (2017).
3. S. Archibald, C. E. R. Lehmann, J. L. Gómez-Dans, R. A. Bradstock, Defining pyromes and global syndromes of fire regimes. *Proceedings of the National Academy of Sciences* **110**, 6442-6447 (2013).
4. M. A. Moritz *et al.*, Learning to coexist with wildfire. *Nature* **515**, 58-66 (2014).
5. D. M. J. S. Bowman, J. J. Sharples, Taming the flame, from local to global extreme wildfires. *Science* **381**, 616-619 (2023).
6. J. T. Abatzoglou, A. P. Williams, R. Barbero, Global Emergence of Anthropogenic Climate Change in Fire Weather Indices. *Geophysical Research Letters* **46**, 326-336 (2019).
7. Y. Zhuang, R. Fu, B. D. Santer, R. E. Dickinson, A. Hall, Quantifying contributions of natural variability and anthropogenic forcings on increased fire weather risk over the western United States. *Proceedings of the National Academy of Sciences* **118**, e2111875118 (2021).
8. A. Barkhordarian, S. S. Saatchi, A. Behrangi, P. C. Loikith, C. R. Mechoso, A Recent Systematic Increase in Vapor Pressure Deficit over Tropical South America. *Scientific Reports* **9**, 15331 (2019).
9. T. M. Ellis, D. M. J. S. Bowman, P. Jain, M. D. Flannigan, G. J. Williamson, Global increase in wildfire risk due to climate-driven declines in fuel moisture. *Global Change Biology* **28**, 1544-1559 (2022).
10. P. Jain, D. Castellanos-Acuna, S. C. P. Coogan, J. T. Abatzoglou, M. D. Flannigan, Observed increases in extreme fire weather driven by atmospheric humidity and temperature. *Nature Climate Change* **12**, 63-70 (2022).
11. W. M. Jolly *et al.*, Climate-induced variations in global wildfire danger from 1979 to 2013. *Nature Communications* **6**, 7537 (2015).
12. L. T. Kelly *et al.*, Understanding Fire Regimes for a Better Anthropocene. *Annual Review of Environment and Resources* **48**, 207-235 (2023).
13. M.-A. Parisien *et al.*, Abrupt, climate-induced increase in wildfires in British Columbia since the mid-2000s. *Communications Earth & Environment* **4**, 309 (2023).
14. J. G. Canadell *et al.*, Multi-decadal increase of forest burned area in Australia is linked to climate change. *Nature Communications* **12**, 6921 (2021).
15. Z. A. Holden *et al.*, Decreasing fire season precipitation increased recent western US forest wildfire activity. *Proceedings of the National Academy of Sciences* **115**, E8349-E8357 (2018).
16. M. W. Jones *et al.*, Global and Regional Trends and Drivers of Fire Under Climate Change. *Reviews of Geophysics* **60**, e2020RG000726 (2022).
17. C. X. Cunningham, G. J. Williamson, D. M. J. S. Bowman, Increasing frequency and intensity of the most extreme wildfires on Earth. *Nature Ecology & Evolution*, (2024).
18. M. Zubkova, M. L. Humber, L. Giglio, Is global burned area declining due to cropland expansion? How much do we know based on remotely sensed data? *International Journal of Remote Sensing* **44**, 1132-1150 (2023).
19. A. Modaresi Rad *et al.*, Human and infrastructure exposure to large wildfires in the United States. *Nature Sustainability*, (2023).

20. V. C. Radeloff *et al.*, Rising wildfire risk to houses in the United States, especially in grasslands and shrublands. *Science* **382**, 702-707 (2023).
21. V. C. Radeloff *et al.*, Rapid growth of the US wildland-urban interface raises wildfire risk. *Proceedings of the National Academy of Sciences* **115**, 3314-3319 (2018).
22. F. Schug *et al.*, The global wildland–urban interface. *Nature* **621**, 94-99 (2023).
23. S. H. Doerr, C. Santín, Global trends in wildfire and its impacts: perceptions versus realities in a changing world. *Philosophical Transactions of the Royal Society B: Biological Sciences* **371**, 20150345 (2016).
24. Munich Re, Topics Geo: Natural Catastrophes 2016. (Munich Reinsurance Company, Munich, Germany). (2017).
25. M. Re, Topics Geo: Natural Catastrophes 2017. (Munich Reinsurance Company, Munich, Germany). (2018).
26. E. Faust, M. Steuer, New hazard and risk level for wildfires in California and worldwide (Munich Reinsurance Company, Munich, Germany). (2019).
27. M. E. González, A. D. Syphard, A. P. Fischer, A. A. Muñoz, A. Miranda, Chile's Valparaíso hills on fire. *Science* **383**, 1424-1424 (2024).
28. C. X. Cunningham *et al.*, Pyrogeography in flux: Reorganization of Australian fire regimes in a hotter world. *Global Change Biology* **30**, e17130 (2024).
29. Munich Re, NatCatSERVICE Methodology. (2018).
30. CRED, UCLouvain. (2023).
31. M. Coronese, F. Lamperti, K. Keller, F. Chiaromonte, A. Roventini, Evidence for sharp increase in the economic damages of extreme natural disasters. *Proceedings of the National Academy of Sciences* **116**, 21450-21455 (2019).
32. J. McLennan, B. Ryan, C. Bearman, K. Toh, Should We Leave Now? Behavioral Factors in Evacuation Under Wildfire Threat. *Fire Technology* **55**, 487-516 (2019).
33. C. A. Kolden, C. Henson, A Socio-Ecological Approach to Mitigating Wildfire Vulnerability in the Wildland Urban Interface: A Case Study from the 2017 Thomas Fire. *Fire*. 2019 (10.3390/fire2010009).
34. The World Bank, The cost of fire: an economic analysis of Indonesia's 2015 fire crisis. (2016).
35. F. H. Johnston *et al.*, Unprecedented health costs of smoke-related PM2.5 from the 2019–20 Australian megafires. *Nature Sustainability* **4**, 42-47 (2021).
36. S. N. Koplitz *et al.*, Public health impacts of the severe haze in Equatorial Asia in September–October 2015: demonstration of a new framework for informing fire management strategies to reduce downwind smoke exposure. *Environmental Research Letters* **11**, 094023 (2016).
37. Center for International Earth Science Information Network - CIESIN - Columbia University, Gridded Population of the World, Version 4 (GPWv4): Population Density, Revision 11. (2018).
38. D. M. J. S. Bowman *et al.*, Human exposure and sensitivity to globally extreme wildfire events. *Nature Ecology & Evolution* **1**, 0058 (2017).
39. J. T. Abatzoglou, A. P. Williams, Impact of anthropogenic climate change on wildfire across western US forests. *Proceedings of the National Academy of Sciences* **113**, 11770-11775 (2016).
40. P. T. Brown *et al.*, Climate warming increases extreme daily wildfire growth risk in California. *Nature* **621**, 760-766 (2023).
41. M. Goss *et al.*, Climate change is increasing the likelihood of extreme autumn wildfire conditions across California. *Environmental Research Letters* **15**, 094016 (2020).
42. J. T. Abatzoglou *et al.*, Downslope Wind-Driven Fires in the Western United States. *Earth's Future* **11**, e2022EF003471 (2023).
43. J. K. Balch *et al.*, Warming weakens the night-time barrier to global fire. *Nature* **602**, 442-448 (2022).

44. K. Luo, X. Wang, M. de Jong, M. Flannigan, Drought triggers and sustains overnight fires in North America. *Nature* **627**, 321-327 (2024).
45. L. R. Hawkins, J. T. Abatzoglou, S. Li, D. E. Rupp, Anthropogenic Influence on Recent Severe Autumn Fire Weather in the West Coast of the United States. *Geophysical Research Letters* **49**, e2021GL095496 (2022).
46. P. E. Higuera *et al.*, Shifting social-ecological fire regimes explain increasing structure loss from Western wildfires. *PNAS Nexus* **2**, pgad005 (2023).
47. G. Mantero *et al.*, The influence of land abandonment on forest disturbance regimes: a global review. *Landscape Ecology* **35**, 2723-2744 (2020).
48. D. M. Bowman *et al.*, Human–environmental drivers and impacts of the globally extreme 2017 Chilean fires. *Ambio* **48**, 350-362 (2019).
49. D. M. J. S. Bowman *et al.*, Vegetation fires in the Anthropocene. *Nature Reviews Earth & Environment* **1**, 500-515 (2020).
50. AON, Weather, Climate & Catastrophe Insight: 2018 Annual Report. (2019).
51. C. Flavelle, J. Cowan, I. Penn, in *New York Times*. (2023).
52. E. J. Xu, C. Webb, D. D. Evans, "Wildfire catastrophe models could spark the changes California needs. Milliman White Paper," (2019).
53. N. Lambrou, C. Kolden, A. Loukaitou-Sideris, E. Anjum, C. Acey, Social drivers of vulnerability to wildfire disasters: A review of the literature. *Landscape and Urban Planning* **237**, 104797 (2023).
54. R. L. Jones, D. Guha-Sapir, S. Tubeuf, Human and economic impacts of natural disasters: can we trust the global data? *Scientific Data* **9**, 572 (2022).
55. M. Burke *et al.*, The changing risk and burden of wildfire in the United States. *Proceedings of the National Academy of Sciences* **118**, e2011048118 (2021).
56. W. Mattioli *et al.*, Estimating wildfire suppression costs: a systematic review. *International Forestry Review* **24**, 15-29 (2022).
57. C. A. Kolden, J. T. Abatzoglou, M. W. Jones, P. Jain, Wildfires in 2023. *Nature Reviews Earth & Environment* **5**, 238-240 (2024).
58. E. E. Knapp, Y. S. Valachovic, S. L. Quarles, N. G. Johnson, Housing arrangement and vegetation factors associated with single-family home survival in the 2018 Camp Fire, California. *Fire Ecology* **17**, 25 (2021).
59. J. R. Arévalo, A. Naranjo-Cigala, Wildfire Impact and the “Fire Paradox” in a Natural and Endemic Pine Forest Stand and Shrubland. *Fire*. 2018 (10.3390/fire1030044).
60. M. R. Kreider *et al.*, Fire suppression makes wildfires more severe and accentuates impacts of climate change and fuel accumulation. *Nature Communications* **15**, 2412 (2024).
61. R. J. Burby, Hurricane Katrina and the Paradoxes of Government Disaster Policy: Bringing About Wise Governmental Decisions for Hazardous Areas. *The ANNALS of the American Academy of Political and Social Science* **604**, 171-191 (2006).
62. D. E. Calkin *et al.*, Wildland-urban fire disasters aren’t actually a wildfire problem. *Proceedings of the National Academy of Sciences* **120**, e2315797120 (2023).
63. S. Ondei, O. F. Price, D. M. J. S. Bowman, Garden design can reduce wildfire risk and drive more sustainable co-existence with wildfire. *npj Natural Hazards*, (2024 In Press).
64. A. D. Syphard, T. J. Brennan, J. E. Keeley, The importance of building construction materials relative to other factors affecting structure survival during wildfire. *International Journal of Disaster Risk Reduction* **21**, 140-147 (2017).
65. A. D. Syphard, J. E. Keeley, Factors Associated with Structure Loss in the 2013–2018 California Wildfires. *Fire*. 2019 (10.3390/fire2030049).
66. M. K. Anderson, The use of fire by Native Americans in California. *Fire in California’s ecosystems. University of California Press, Berkeley, California, USA*, 417-430 (2006).
67. K. McConnell, L. Koslov, Critically assessing the idea of wildfire managed retreat. *Environmental Research Letters* **19**, 041005 (2024).

68. V. Steffensen. (CSIRO Publishing, 2020).
69. M. Mariani *et al.*, Disruption of cultural burning promotes shrub encroachment and unprecedented wildfires. *Frontiers in Ecology and the Environment* **20**, 292-300 (2022).
70. X. Wu, E. Sverdrup, M. D. Mastrandrea, M. W. Wara, S. Wager, Low-intensity fires mitigate the risk of high-intensity wildfires in California's forests. *Science Advances* **9**, eadi4123 (2023).
71. E. G. Brodie, E. E. Knapp, W. R. Brooks, S. A. Drury, M. W. Ritchie, Forest thinning and prescribed burning treatments reduce wildfire severity and buffer the impacts of severe fire weather. *Fire Ecology* **20**, 17 (2024).
72. E. L. Kalies, L. L. Yocom Kent, Tamm Review: Are fuel treatments effective at achieving ecological and social objectives? A systematic review. *Forest Ecology and Management* **375**, 84-95 (2016).
73. K. T. Davis *et al.*, Tamm review: A meta-analysis of thinning, prescribed fire, and wildfire effects on subsequent wildfire severity in conifer dominated forests of the Western US. *Forest Ecology and Management* **561**, 121885 (2024).
74. J. M. Furlaud, G. J. Williamson, D. M. J. S. Bowman, Mechanical treatments and prescribed burning can reintroduce low-severity fire in southern Australian temperate sclerophyll forests. *Journal of Environmental Management* **344**, 118301 (2023).
75. A. Wirtz, W. Kron, P. Löw, M. Steuer, The need for data: natural disasters and the challenges of database management. *Natural Hazards* **70**, 135-157 (2014).
76. AON, 2022 Weather, Climate and Catastrophe Insight. (2023).
77. AON, 2021 Weather, Climate and Catastrophe Insight. (2022).
78. AON, Weather, Climate & Catastrophe Insight: 2020 Annual Report. (2021).
79. AON, Weather, Climate & Catastrophe Insight: 2019 Annual Report. (2020).
80. D. Delforge *et al.*, EM-DAT: the Emergency Events Database. (2023).
81. R. L. Jones, A. Kharb, S. Tubeuf, The untold story of missing data in disaster research: a systematic review of the empirical literature utilising the Emergency Events Database (EM-DAT). *Environmental Research Letters* **18**, 103006 (2023).
82. A. L. Mahood, E. J. Lindrooth, M. C. Cook, J. K. Balch, Country-level fire perimeter datasets (2001–2021). *Scientific Data* **9**, 458 (2022).
83. USDA Forest Service/US Geological Service. (2024).
84. R. J. Hall *et al.*, Generating annual estimates of forest fire disturbance in Canada: the National Burned Area Composite. *International Journal of Wildland Fire* **29**, 878-891 (2020).
85. G. Ryu, C. Charalambou. (2023).
86. S. Muff, E. B. Nilsen, R. B. O'Hara, C. R. Nater, Rewriting results sections in the language of evidence. *Trends in Ecology & Evolution*, (2021).
87. E. Dinerstein *et al.*, An Ecoregion-Based Approach to Protecting Half the Terrestrial Realm. *BioScience* **67**, 534-545 (2017).
88. R. Valavi, G. Guillera-Arroita, J. J. Lahoz-Monfort, J. Elith, Predictive performance of presence-only species distribution models: a benchmark study with reproducible code. *Ecological Monographs* **n/a**, e1486 (2021).
89. M. Barbet-Massin, F. Jiguet, C. H. Albert, W. Thuiller, Selecting pseudo-absences for species distribution models: how, where and how many? *Methods in Ecology and Evolution* **3**, 327-338 (2012).
90. MODIS Collection 6 Hotspot / Active Fire Detections MCD14ML distributed from NASA FIRMS. Available on-line https://earthdata.nasa.gov/firms. doi:10.5067/FIRMS/MODIS/MCD14ML.
91. L. Giglio, J. Descloitres, C. O. Justice, Y. J. Kaufman, An Enhanced Contextual Fire Detection Algorithm for MODIS. *Remote Sensing of Environment* **87**, 273-282 (2003).
92. L. Giglio, R. L. Schroeder, J. V. Hall, C. Justice, MODIS Collection 6 and Collection 6.1 Active Fire Product User's Guide. NASA. (2021).

93. U. Nations, Methodology: standard counrty or area codes for statistical use (M49). URL: https://unstats.un.org/unsd/methodology/m49. Accessed on 6 May 2024. (2024).
94. S. N. Wood, *Generalized Additive Models: An Introduction with R (2nd ed.)*. (CRC Press, Boca Raton, FL, USA, 2017).
95. R Core Team. (R Foundation for Statistical Computing, Vienna, Austria, 2023).
96. O. Allouche, A. Tsoar, R. Kadmon, Assessing the accuracy of species distribution models: prevalence, kappa and the true skill statistic (TSS). *Journal of Applied Ecology* **43**, 1223-1232 (2006).
97. H. Hersbach *et al.*, The ERA5 global reanalysis. *Quarterly Journal of the Royal Meteorological Society* **146**, 1999-2049 (2020).
98. C. Vitolo *et al.*, ERA5-based global meteorological wildfire danger maps. *Scientific Data* **7**, 216 (2020).
99. W. C. Palmer, Meteorological drought. US. *Weather Bureau Res. Paper* **45**, 1-58 (1965).
100. R. G. Allen, L. S. Pereira, D. Raes, M. Smith, FAO Irrigation and drainage paper No. 56. *Rome: Food and Agriculture Organization of the United Nations* **56**, e156 (1998).

Acknowledgments

Funding: This research was funded by the Australian Research Council (FL220100099) to DMJSB. CAK was supported by USDA NIFA (2022-67019-36435). JTA was supported by NSF award OAI-2019762.

Author contributions:

Conceptualization: DMJSB;
Methodology: CXC, JTA, GJW, CAK, DMJSB;
Data: MS, CXC;
Investigation: CXC, JTA;
Visualization: CXC;
Funding acquisition: DMJSB;
Supervision: DMJSB;
Writing – original draft: CXC;
Writing – review & editing: CXC, DMJSB, CAK, JTA, GJW, MS.

Competing interests: The authors declare no competing interests.

Data and materials availability:

Data as described below and code are available for peer review at a journal and will be archived at a permanent repository upon acceptance. These data and code allow reproduction of all analyses except for Fig 1c-e because providing those data would violate our contractual obligations with Munich Re.

We provide the original EM-DAT dataset used, which is also publicly available at https://www.emdat.be/.

The NatCatSERVICE dataset was provided to us in 2018 by Münchener Rückversicherungs-Gesellschaft (Munich Reinsurance Company) under a contractual condition prohibiting us from sharing this commercially confidential dataset. In 2024, Munich Re provided us with updated estimates for the years 1980-2018. We thank Munich Re for making the dataset available for this analysis. We have attempted to make available the fullest version of the harmonised EM-DAT/NatCatSERVICE dataset in pursuit of open data while adhering to our contractual obligations. We have thus made the harmonised dataset available, with loss estimates redacted when based solely on Munich Re; importantly, the combined dataset contains a column denoting whether the event was a major or minor event, thus facilitating reproduction of most analyses.

The time series of metrics derived from ERA5 climate data are provided for each major disaster location.

We acknowledge the use of MODIS active fire data from the Fire Information for Resource Management System (FIRMS; https://earthdata.nasa.gov/firms). We have provided annual maps of summarised fire metrics used in the distribution model.

Supplementary Material

Methods:

Data

(i) Disaster data

We compiled a dataset of wildfire disasters primarily by integrating the two most comprehensive global databases on the direct economic losses and fatalities associated with disasters: NatCatSERVICE (1980-2017) and Emergency Events Database (EM-DAT; 1980-2023). NatCatSERVICE is compiled by the global reinsurer, Munich Re, who are experts in damage estimation. This dataset is not publicly available and was provided to us under restricted use. While systematic data collection began in 1974, Munich Re state that only data from 1980 onwards is suitable for systematic analysis (*29, 75*). In addition to fatalities and damages (USD), NatCatSERVICE categorises direct economic damages onto 0-6 scale based on a country's cost of living using World Bank income groups, with class 2 corresponding to "moderate" (for details, see *29*). We did not have access to NatCatSERVICE from 2019 onwards; for 2019 onwards, we additionally used AON's annual reports of catastrophe events (*50, 76-79*), which collate information on natural catastrophes in a systematic way comparable to NatCatSERVICE.

Since its creation in 1988, EM-DAT has provided a publicly available record of disasters compiled from systematic evaluation of sources from UN agencies, non-governmental organizations, reinsurance companies, research institutes, and press agencies (*30, 80*). It focuses on major societal disasters, with at least one of the following thresholds required for inclusion in the dataset: (i) 10 fatalities, (ii) 100 affected people, (iii) a declaration of state of emergency, or (iv) a call for international assistance (*30*).

Given all disaster databases suffer from some degree of bias, missing information (e.g., missing damage estimates), absent events (especially small ones), and disparities in damage estimates (*54, 81*), there was a need to harmonise the datasets into a single dataset (see Fig S1 for workflow and Fig S2 for dataset comparison). Because EM-DAT is publicly available, frequently updated, and is intended for scientific use, we used it as the base dataset and modified it when NatCatSERVICE:

(i) provided information on significant disaster events (disaster class ≥ 2) that were not included in EM-DAT, in which case we added these events.
(ii) indicated significant discrepancies between direct losses, in which case we searched reports from government agencies, non-governmental organisations, and news agencies, and/or contacted both dataset managers to seek clarification.
(iii) disaggregated events into finer-scale components, in which case we used the finest spatial disaggregation available.

All damage costs were converted from US dollars in the year of the disaster to 2022 US dollars using the consumer price index recorded in EM-DAT. Despite converting to a common price, the null expectation should be that more recent years will have larger damage costs because the economy is larger in real terms (partly due to population growth). Furthermore, damage in US dollars does not account for differences in prices among countries. Thus, to account for different economic scales across countries, we converted economic losses from nominal values (US dollars in disaster year) to losses as a percentage of a country's GDP for the same year. This method standardizes the economic impact relative to the sizes and prices of each economy, providing a comparable measure of the extent to which an economy can absorb the disaster losses. For GDP, we used estimated national GDP from the World Bank (https://databank.worldbank.org/reports.aspx?source=2&series=NY.GDP.MKTP.CD&country), and imputed values for country-years with missing data (6%).

After calculating relative disaster costs (% of GDP), we used the 200 most economically damaging events and those that caused 10 or more fatalities for further analysis. While this threshold of 200 events is somewhat arbitrary, it provides a tractable and substantial georeferenced dataset of the most disastrous events since 1980. Importantly, it provides a means of comparing the relative magnitude and frequency of major disasters through time and among economies with different currencies and prices. Doing so has the benefit of focusing on major events that would suffer minimal reporting bias through time, which is an important consideration given the increasing ease of communication following the advent of the internet. Combining these major economic and major fatality disasters resulted in a dataset of 242 major wildfire disasters; of these, 43 were joint major economic and fatality events, 157 were major economic events only, and 42 were major fatality events only.

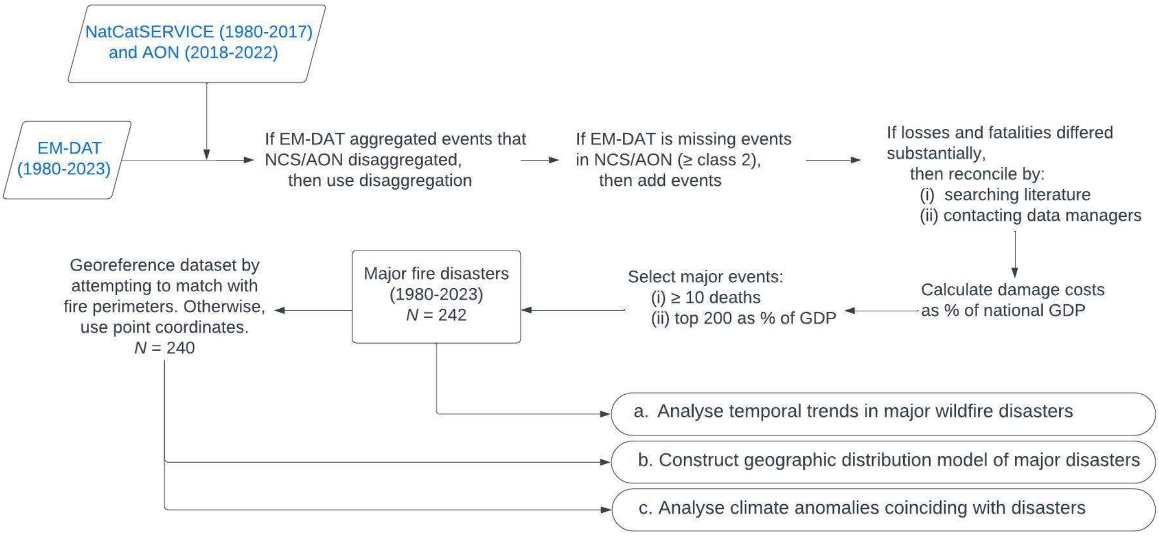

Figure S1. Workflow of harmonising global disaster datasets. *Main steps involved in harmonising and analysing major wildfire disasters.*

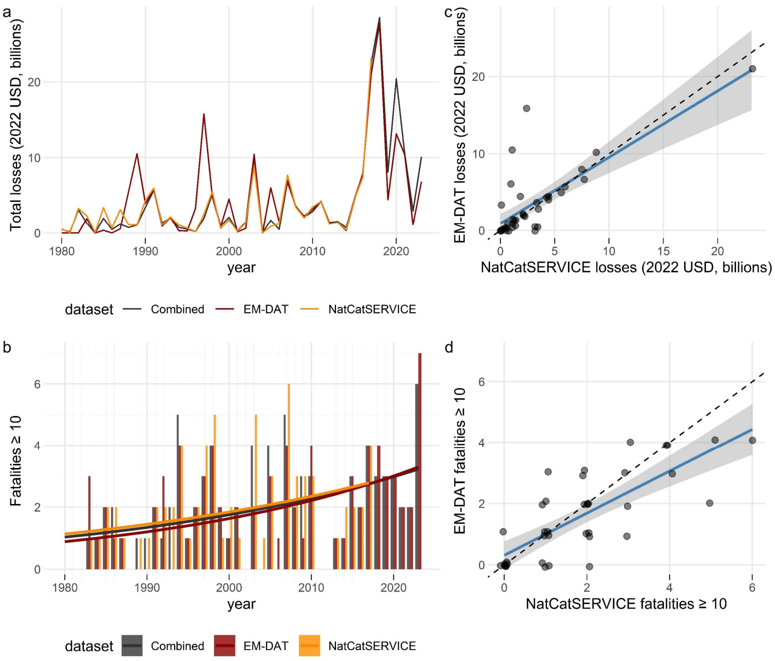

Figure S2. Comparing global disaster datasets. (a-b) *Time series of the total losses and number of major fatality events (>= 10 fatalities) recorded by the datasets. Lines in b show the fits of generalised linear models.* ***(c-d)*** *Comparison of the total loss estimates and number of major fatality events, with each point representing one year. The dashed line shows a 1:1 line, while the blue line shows a linear regression.*

(ii) *Geolocating the major disaster events*

EM-DAT does not contain spatial coordinates, only locality names. NatCatSERVICE records point coordinates along with a detailed description of the affected locations and sometimes wildfire names. The spatial matching process therefore required additional research using news and government agency reports to identify specific locations affected by the disasters.

Where possible, we attempted to match the major disasters with polygon(s) of the area burned by the relevant fires. To do this, we used a combination of satellite-derived products, specifically the globally available fire perimeter dataset, Fire Event Delineation (FIRED; *82*), as well as national fire perimeter datasets for the USA (Monitoring Trends in Burn Severity; *83*), Canada (National Burned Area Composite; *84*), and Australia (Historical Bushfire Boundaries; *85*). If matching an event to fire polygons was not possible (e.g., occurred prior to geospatial fire perimeter datasets), we used point coordinates for those disasters. Notably, this spatial matching process involved two common types of wildfire disaster: events involving one or a small number of fires, and diffuse, broad-scale events involving many concurrent fires, such as the tens of thousands of small fires that burned in Indonesia in 2015, culminating in a major humanitarian disaster. For diffuse events, it is difficult to determine which fires caused economic damage and fatalities, and their widespread nature is often a key feature that overwhelms fire-fighting capacity. In these cases, we included all fires in the reported region within the relevant date range. The spatial point or polygon matching was possible for 240 of 242 disasters in the final dataset.

Statistical analysis

(i) *Temporal trends of wildfire disasters*

We constructed and analysed temporal trends in five metrics that characterise various dimensions of wildfire disasters (Table S1): (1) frequency of economic disasters, (2) frequency of major fatality events, (3) total annual damage costs, (4) total damage costs as a percentage of global GDP, and (5) frequency of billion-dollar events. We present fits of statistical models as well as 5-year moving averages, and interpret model coefficients and p-values as continuous rather than binary measures of evidence (recommended by *86*).

First, we analysed the annual count of major disaster events using the 200 most damaging events, calculated as a share of GDP as described in the previous section (model 1a, Table S1). We fitted this model using a generalised linear model (GLM) with negative binomial distribution, with the annual global count of disasters modelled in response to year (1980-2023). To further investigate whether trends differed regionally, we fitted a GLM with each geographic region's count of disasters modelled in response to a region × year interaction (model 1b, Table S1). We tested the importance of the interaction using AIC by comparing the interactive model with a simpler model with additive effects of region and year.

Second, we modelled the annual count of major fatality events, defined as wildfire events leading to at least 10 fatalities (model 2, Table S1). This represents a relatively high threshold for wildfire disasters, but it corresponds with EM-DAT's threshold, providing a standardised metric to evaluate changes in the frequency of major fatality events. Further, it is likely that events of this threshold would suffer minimal reporting bias, as they are unambiguously disastrous wildfires that are likely to be reported on widely.

Third, we analysed total annual damage costs (2022 USD) from all disasters in the harmonised dataset (not just the top 200; model 3, Table S1).

Fourth, we analysed changes in total annual damage costs as a percentage of time-matched global GDP (model 4, Table S1). Because temporal trends in both of these metrics were strongly non-linear (Fig 1d-e), we report changes in the 5-year moving average rather than fit a statistical model.

Fifth, we used a GLM with negative binomial distribution to model the frequency of billion-dollar events (in 2022 USD) in response to a linear effect of year.

Table S1. Summary of approaches used to analyse temporal change in different metrics of wildfire disasters.

model#	response variable	structure	type
1a	economic disasters globally (annual count)	~ year	GLM
1b	economic disasters in each region (annual count)	~ year × region ~ year + region	GLM
2	major fatality events (annual count)	~ year	GLM
3	total annual damage costs (2022 USD)	~ year	moving average
4	total annual damage costs (% of global GDP)	~ year	moving average
5	billion-dollar events (annual count)	~ year	GLM

(ii) Geographic distribution of major disasters

To broadly summarise the geographic distribution of major disasters, we calculated the ratio of disasters occurring in the Earth's biomes relative to the area and population size of each biome (*87*). We calculated the ratio by dividing the percentage of disasters occurring in each biome (*87*) by (i) the percentage of Earth's land covered by each biome (excluding snow/ice covered biomes, such as Antarctica), and (ii) the percentage of the global population living in each biome based on the nearest year available (1990, 1995, 2000, 2005, 2015, 2020; Gridded Population of the World v3 and v4 (*37*)). Ratios above 1 indicate that disasters occurred at a higher rate than expected based on the biome areas or population sizes.

Next, to statistically investigate the pyrogeographic distribution of major disasters, we constructed statistical models that distinguished disaster locations from background locations. Using background locations to characterise the available domain in which disasters could occur is the same approach commonly used to model species distributions from presence-only data (*88, 89*), and provides the analogous prediction of the locations in which fire disasters are most likely to occur. To adequately characterise available environmental space, Barbet-Massin et al. (*89*) recommend distributing at least 10,000 background points. We therefore randomly distributed 100 background locations for every major disaster, totalling 24,000 background locations. Background points were randomly distributed over the entire Earth (except Antarctica). As recommended (*36*), we fitted the model with background locations down-weighted, such that the sum of disaster weights equalled the sum of available location weights (i.e., disasters had weights of 1 and background locations had weights of 1/100). Disaster and background locations were labelled with 7 explanatory variables (Fig S3):

(1) population density (people/km^2) of each 0.25° cell using version 4.11 of the Gridded Population of the World dataset (*37*). We used the year 2000 as the approximate mid-point of the study.

(2-3) summed fire radiative power using day and night hotspots (ΣFRP) and summed fire radiative power using night hotspots only ($\Sigma \mathrm{FRP}_{night}$). We calculated these using MODIS active fire records (MCD14ML product), which include the locations of observed fires at a spatial resolution of 1 km (*90, 91*). Each hotspot is accompanied by a measure of fire radiative power (MW), which has been widely used as a proxy of fire intensity. We excluded low-confidence observations (i.e., confidence < 30; *92*), and calculated summed FRP

(MW/km^2) at a spatial resolution of 0.25° for each year from 2003-2023, of which we then calculated the cell-wise mean.

(4-5) hotspot density (using day and night hotpots), and nighttime hotspot density (using night hotspots only). We calculated these by summing the number of MODIS hotspots occurring in each 0.25° cell for each year from 2003-2023, and then dividing by the area (km^2) of the cell.

(6) geographic region, following continent designations used by the United Nations geoscheme (*93*) e.g., Russia is described as part of eastern Europe even though it spans both northern Asia and eastern Europe (Fig S3). Since our focus of the analysis was societally disastrous wildfires, we considered the UN definition a reasonable practical choice because much of Russia is culturally more like Europe than Asia.

(7) biome, using the Earth's 14 terrestrial biomes (Fig S3) delineated by Dinerstein et al. (*87*).

Continuous variables (fire variables and population density) were log-transformed before being used in a generalised additive model (GAM), fitted with binomial distribution using the mgcv package v1.8-42 (*94*) in R v4.3.0 (*95*). GAMs are like generalised linear models (GLM) except they allow flexible fitting of non-linear relationships if supported by the data (*94*). The model algorithm penalises parameter complexity, automatically selecting the optimal degree of smoothing supported by the data. We constructed a series of competing GAMs involving different combinations of the above variables (see Table S5 for full model set). The most complex model took the form:

$$\mathit{Disaster} \sim \mathit{ti(logFire, logPop)} + \mathit{ti(logFire)} + \mathit{ti(logPop)} + \mathit{biome} + \mathit{region}$$

where *logFire* refers to one of the four abovementioned fire variables, *ti(logFire, logPop)* is a tensor product interaction between log-transformed fire variable and log-transformed population; *ti(logFire)* and *ti(logPop)* are the main effects of those variables, and *biome* and *region* are categorical effects.

We evaluated the performance of the different models using k-fold cross-validation with 10 folds. Model performance was evaluated based on the average model ranks using four criteria: (i) Akaike's information criterion (AIC); (ii) mean area under the receiver operating characteristic curve (AUC_{ROC}) calculated on the withheld folds of data; (iii) the true skill score, which incorporates sensitivity and specificity (*96*), calculated using the withheld folds of data; and (iv) deviance explained.

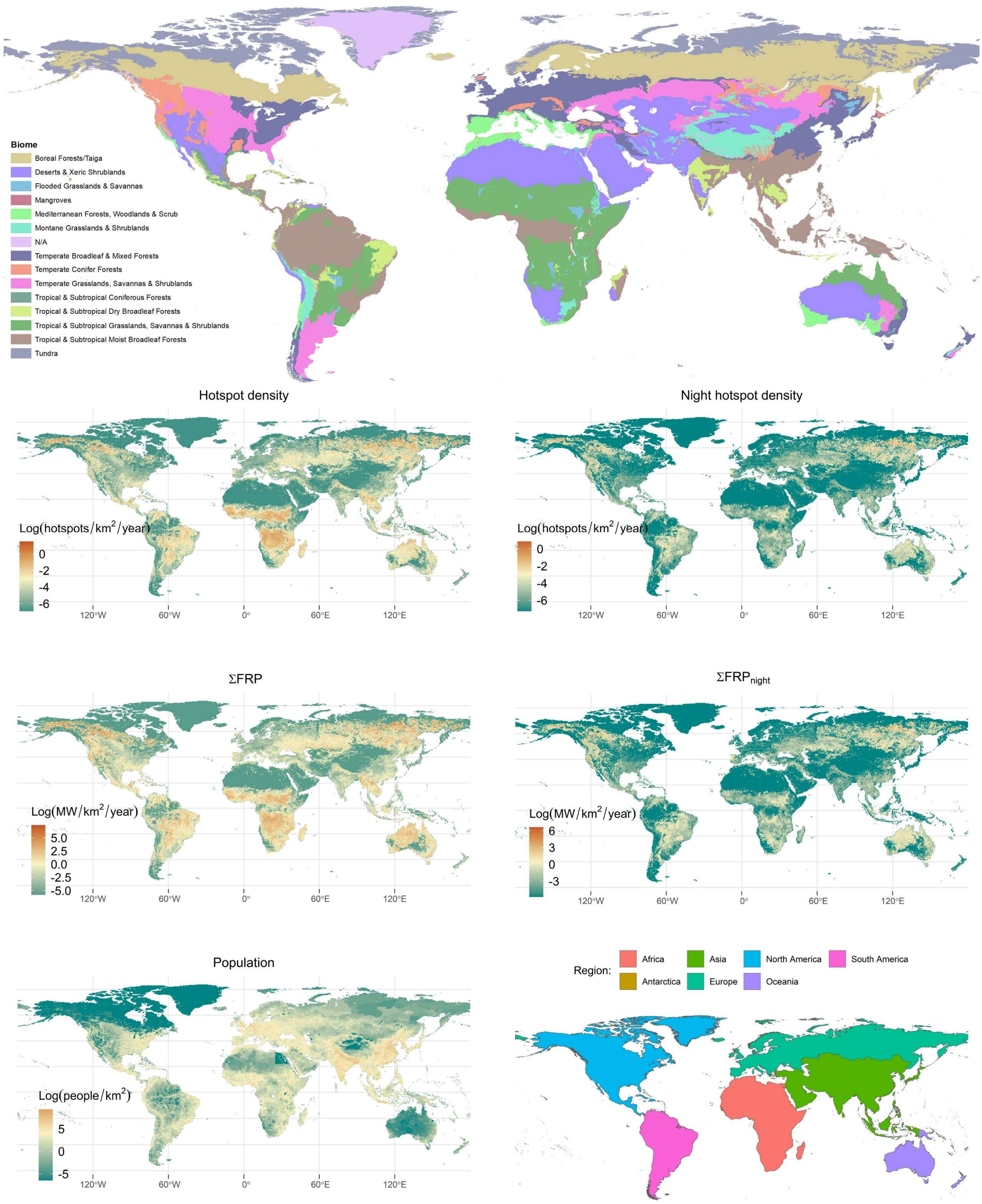

Figure S3. Explanatory variables used in the analysis of the distribution of wildfire disasters. *Biomes follow the delineation by Dinerstein et al. (87), the shapefile of which was downloaded from [https://ecoregions.appspot.com/.](https://ecoregions.appspot.com/) Geographic regions follow the continent definitions used by United Nations geoscheme (93), whereby Russia is described as part of eastern Europe even though it spans both northern Asia and eastern Europe. Fire metrics were calculated based on MODIS active fire "hotspots" from 2003-2023.*

(iii) *Climatic correlates of wildfire disasters*

We analysed the association between major wildfire disasters and three key interrelated climatological measures: fire weather index (FWI), measuring the potential for fire spread; vapor pressure deficit (VPD), indicating the air's short-term capacity to dry fuels; and Palmer drought severity index (PDSI [inverted by multiplying by -1]), reflecting longer-term drought stress. Data were derived from ERA-5, a modern reanalysis at a 0.25-degree horizontal resolution (*97*) that have been widely used in global climate and fire weather studies. Daily FWI from the Canadian Forest Fire Danger Rating System is sourced from ERA-5, integrating the influence of longer-term fuel drying and short-term fire weather conditions (*98*). Daily VPD is calculated from hourly temperature and dewpoint temperature from ERA-5. Lastly, monthly PDSI is calculated following the water balance approach of (*99*) from ERA-5 precipitation as well as reference evapotranspiration derived from the Penman-Monteith formula (*100*).

We quantified fire weather and drought anomalies coinciding with the disasters relative to conditions for the same period of other years from 1979-2023. To do this, we identified the Julian day periods of each disaster's wildfire (± 1 day) ("fire period" in Fig S4, step 1a). For FWI and VPD, we identified the most extreme day within the Julian day fire period each year, which we refer to as FWI_{max} and VPD_{max} (Fig S4, step 1a-b). For monthly PDSI, we used the month of ignition in the disaster year and compared it to the same month in non-disaster years.

For each disaster location separately, all values were then transformed to standard deviations (i.e., z-score standardisation) by subtracting the mean and dividing by the standard deviation (Fig S4, step 1c), providing a standardised measure of the departure from the average time-matched extreme. We visualised relationships using bivariate scatter and density plots, and quantified compound extremes by calculating the percentage of disasters occurring in each quadrant of the bivariate relationships. We used a one-sample t-test to quantify whether the mean anomaly of the 240 disasters differed from the average (i.e., zero) time-matched extreme.

To evaluate how these climatological variables have changed at the disaster locations during the period 1979-2023, we used the 240 values each year (one for each disaster location) to calculate each year's mean anomaly. We then split the study period into two near-equal periods (1979-2000 and 2001-2023) and used a two-sample t-test to evaluate whether the time-matched extremes differed between the periods. To further characterise changes in climatic conditions at the disaster locations, we additionally transformed the full time series (1979-2023) of FWI, VPD, and PDSI to percentiles for each disaster location. We then calculated the proportion of days each year ≥99.8th percentile (which was the median FWI_{max} value during the fire disasters). We modelled the temporal trends in these metrics using a generalised additive model with gamma distribution.

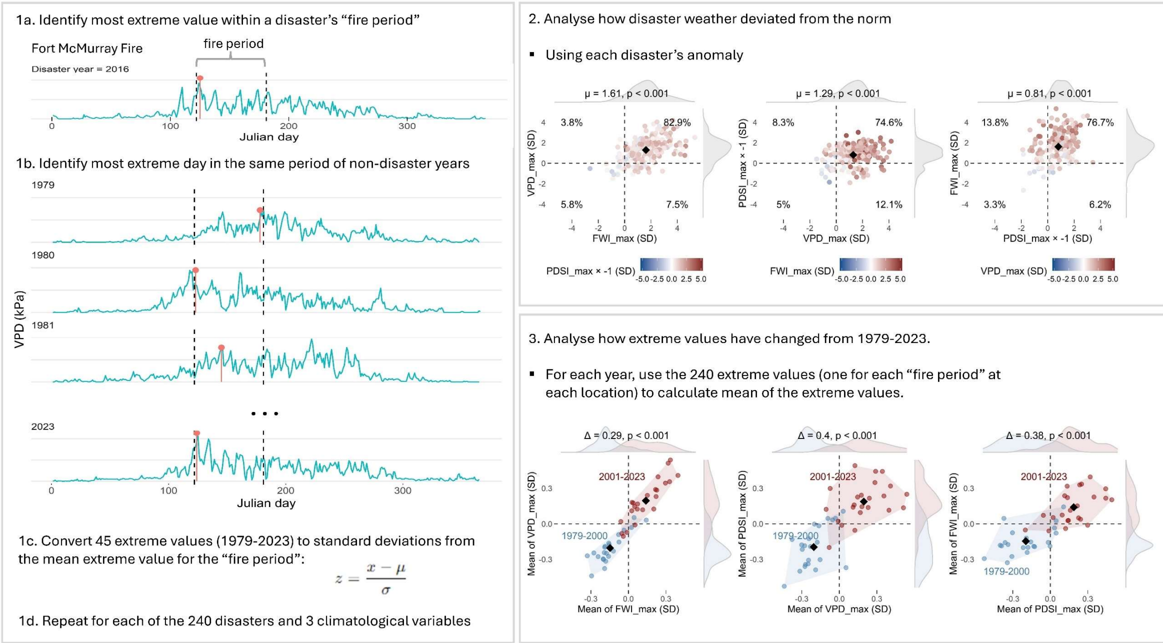

Figure S4. Depiction of the main steps involved in analysing the climatological conditions associated with the major wildfire disasters. *Step 1: For each disaster and year, we selected the most extreme FWI and VPD values within the Julian day period corresponding with the fire (the "fire period"), indicated by the red line and dot. For the monthly PDSI, we selected the value in the ignition month (in all years). These values were then standardized by subtracting the mean and dividing the by standard deviation (separately for each site), providing a standardised measure of the extreme value anomaly relative to typical seasonal extremes. Step 2: to evaluate compound extremes, we created bivariate scatter and density plots of the anomalies of each disaster and tested whether values differed significantly from the average time-matched extreme (i.e., zero). Step 3: to evaluate how these climatological variables have changed during the period 1979-2023, we calculated the mean of the "fire period" extreme values for each year (resulting in one average anomaly per year) and tested for differences between the periods 1979-2000 and 2001-2023.*

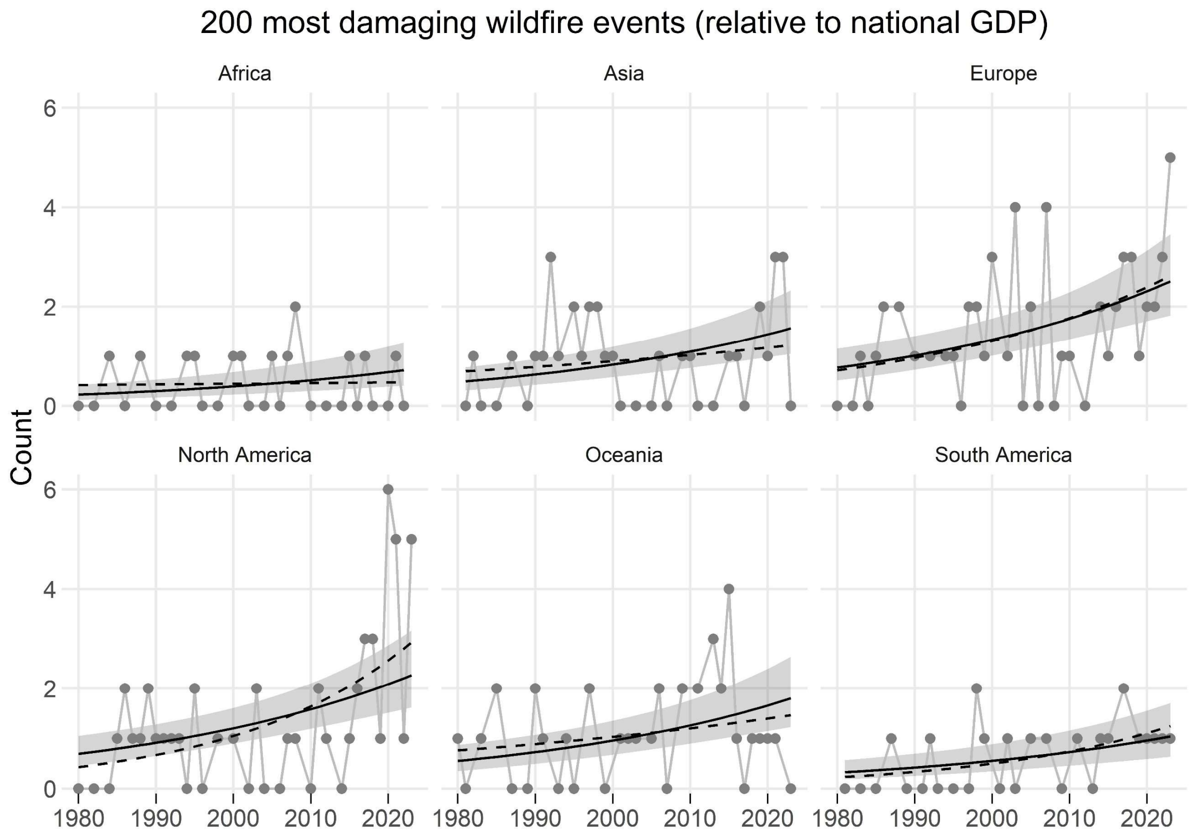

Fig S5. Trends of major economic wildfire disasters among the geographic regions. Major economic disasters were defined as the 200 most damaging wildfires relative to contemporaneous national GDP. The solid line and confidence band shows the fit and 95% CI of the best-performing generalised linear model ($AICc_{weight}$ = 0.95), which did not contain a region by year interaction. The dashed line shows the fit of the second-best GLM ($AICc_{weight}$ = 0.05), which contained a region by year interaction (Table S2).

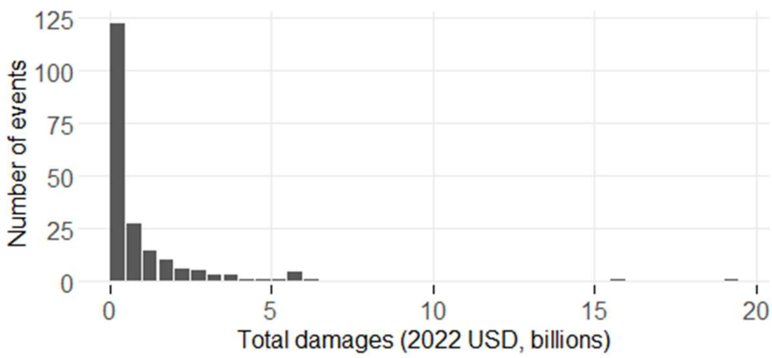

Fig S6. The skewed distribution of economic losses caused by the top 200 most damaging wildfire disasters. A relatively small number of disasters cause the majority of economic losses.

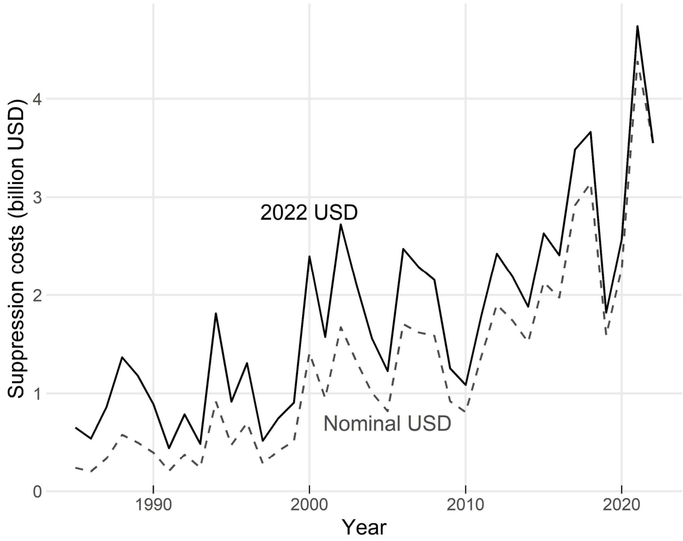

Fig S7. United States federal expenditure on wildfire suppression. We downloaded nominal expenditure (dashed line) from the National Interagency Fire Center (https://www.nifc.gov/fire-information/statistics/suppression-costs), and converted values to 2022 US dollars (solid line) using the consumer price index. The five-year average increased by 3.5-fold between the periods 1985-1989 ($0.92 billion) and 2018-2022 ($3.26 billion),

Table S2. Model selection table for competing generalized linear models of the trend in major economic disasters among the geographic regions. Model fitting began by comparing the most complex (i.e., interactive) model fit with the negative binomial and poisson distributions. The poisson distribution best fit the data (AICc weight = 0.76). Thus, models in this table were all fitted using the poisson distribution. See Fig S5 for the fitted trends of the top two models.

intercept	region	year	region × year	df	logLik	AICc	ΔAICc	weight
-55.91	+	0.027		7	-235.6	485.7	0	0.95
-6.73	+	0.003	+	11	-232.9	491.9	5.7	0.05
-54.76		0.027		1	-249.9	503.9	18.2	0
-0.8	+			6	-247.2	506.9	21.5	0
0.04				0	-261.4	524.8	39.0	0

Table S3. Coefficients from generalized linear models of trends in wildfire disasters. Models are numbered according to the description in table S1.

Model	Variable	Estimate	Std Error	z value	Pr(>|z|)	Deviance explained
1a. Major economic disasters						39.4%
	intercept	-67.7	12.7	-5.34	9.23e-08	
	year	0.0345	0.00631	5.47	4.60e-08	
1b. Major economic disasters by region						22%
	intercept	-55.9	11.7	-4.79	1.64e-06	
	year	0.03	0.00581	4.73	2.24e-06	
	regionAsia	0.751	0.33	2.27	0.023	
	regionEurope	1.22	0.308	3.97	7.2e-05	
	regionNorth America	1.12	0.312	3.6	0.0003	
	regionOceania	0.983	0.326	2.74	0.006	
	regionSouth America	0.345	0.364	0.947	0.343	
2. Major fatality events						14.7%
	intercept	-52.5	18.3	-2.87	0.00415	
	year	0.0265	0.00913	2.91	0.00367	
5. Billion-dollar events						28.7%
	intercept	-105.4	27.3	-3.86	0.0001	
	year	0.052	0.013	3.87	0.0001	

Table S4. Summary of the distribution of major disasters by region and biome. Table shows the number of major economic and fatality disasters occurring in the biomes of each region.

BIOME	Europe	North America	Asia	South America	Africa	Oceania	Total
Mediterranean Forests, Woodlands & Scrub	34	13	9	5	5	11	**77**
Temperate Broadleaf & Mixed Forests	19	3	10	6	0	17	**55**
Temperate Conifer Forests	1	24	4	0	2	0	**31**
Tropical & Subtropical Grasslands, Savannas & Shrublands	0	1	1	6	11	2	**21**
Tropical & Subtropical Moist Broadleaf Forests	0	1	14	0	2	1	**18**
Temperate Grasslands, Savannas & Shrublands	6	3	5	2	0	1	**17**
Boreal Forests/Taiga	7	5	0	0	0	0	**12**
Montane Grasslands & Shrublands	0	0	0	0	2	1	**3**
Flooded Grasslands & Savannas	1	0	0	1	0	0	**2**
Tropical & Subtropical Dry Broadleaf Forests	0	2	0	0	0	0	**2**
Deserts & Xeric Shrublands	0	0	1	0	0	0	**1**
Tropical & Subtropical Coniferous Forests	0	1	0	0	0	0	**1**
Total	**68**	**53**	**44**	**20**	**22**	**33**	**240**

Table S5. Comparisons of competing generalised additive models (GAM) of the distribution of major wildfire disasters relative to background locations. Models were fitted using the binomial distribution. Models were fitted using k-fold cross-validation with 10 folds and evaluated based on the average model ranks using four criteria: Akaike's information criterion (AIC); mean area under the receiver operating characteristic curve (AUC_{ROC}) using the fold of data withheld from model fitting in each iteration; and the true skill score using the withheld fold of data. Model description in the table follows syntax of the mgcv package in R, whereby "*s(x)*" indicates a smooth non-linear function of *x*, "*ti(x,z)*" indicates a tensor product interaction between x and z (in which case main effects are separated using "*ti*(x)" and "*ti(z)*").

model	Average rank	ΔAIC	mean test AUC	mean deviance explained	True skill score
s(ΣFRPnight) + s(log_pop) + biome + region	**2.25**	3.99 (5)	**0.91 (1)**	0.49 (2)	**0.66 (1)**
ti(ΣFRPnight, log_pop) + ti(ΣFRPnight) + ti(log_pop) + biome + region	2.75	3.73 (4)	0.91 (2)	**0.5 (1)**	0.65 (4)
s(log_pop) + s(ΣFRPnight) + biome	3	0.68 (2)	0.9 (3)	0.47 (5)	0.66 (2)
s(log_pop) + s(ΣFRPnight) + region	5	**0 (1)**	0.9 (6)	0.43 (10)	0.65 (3)
ti(log_hs_night_density, log_pop) + ti(log_hs_night_density) + ti(log_pop) + biome + region	5.5	6.95 (7)	0.9 (5)	0.49 (3)	0.63 (7)
s(log_hs_night_density) + s(log_pop) + biome + region	6	7.96 (8)	0.9 (4)	0.48 (4)	0.63 (8)
s(log_pop) + s(log_hs_night_density) + biome	6.5	4.38 (6)	0.9 (7)	0.46 (7)	0.64 (6)
ti(ΣFRP, log_pop) + ti(ΣFRP) + ti(log_pop) + biome + region	8.25	14.23 (13)	0.9 (9)	0.47 (6)	0.64 (5)
s(ΣFRP) + s(log_pop) + biome + region	10	15.92 (15)	0.9 (8)	0.46 (8)	0.63 (9)
s(log_pop) + s(ΣFRP) + biome	10.75	13.7 (12)	0.89 (10)	0.43 (11)	0.62 (10)
s(log_pop) + s(log_hs_night_density) + region	12.5	8 (9)	0.89 (11)	0.4 (19)	0.62 (11)
ti(log_hs_density, log_pop) + ti(log_hs_density) + ti(log_pop) + biome + region	13.5	19.32 (19)	0.89 (12)	0.44 (9)	0.6 (14)
s(log_pop) + s(ΣFRPnight)	13.75	3.73 (3)	0.89 (14)	0.38 (21)	0.59 (17)
s(log_hs_density) + s(log_pop) + biome + region	14.25	19.5 (20)	0.89 (13)	0.43 (12)	0.61 (12)
biome + s(ΣFRPnight)	15	12.15 (11)	0.88 (16)	0.42 (14)	0.58 (19)
s(ΣFRPnight) + biome + region	15.5	18.12 (18)	0.88 (15)	0.43 (13)	0.6 (16)
biome + s(log_hs_night_density)	16.25	15.19 (14)	0.88 (20)	0.41 (16)	0.6 (15)
s(log_pop) + s(ΣFRP) + region	17.75	17.65 (16)	0.88 (17)	0.37 (25)	0.61 (13)
s(log_hs_night_density) + biome + region	18.25	21.28 (22)	0.88 (18)	0.42 (15)	0.58 (18)
s(log_pop) + s(log_hs_density) + biome	18.25	18.03 (17)	0.88 (19)	0.4 (17)	0.57 (20)
s(log_pop) + s(log_hs_night_density)	20.5	12 (10)	0.87 (23)	0.34 (27)	0.56 (22)
s(ΣFRP) + biome + region	21.75	25.84 (24)	0.87 (21)	0.4 (18)	0.56 (24)
biome + s(ΣFRP)	23	21.37 (23)	0.87 (22)	0.39 (20)	0.53 (27)
s(log_pop) + s(ΣFRP)	25.25	20.98 (21)	0.84 (29)	0.3 (30)	0.57 (21)
s(log_pop) + biome + region	25.25	30.27 (28)	0.86 (24)	0.38 (23)	0.54 (26)
s(log_pop) + s(log_hs_density) + region	26	26.63 (26)	0.85 (27)	0.32 (28)	0.56 (23)
s(log_hs_density) + biome + region	26	30.52 (29)	0.86 (25)	0.38 (22)	0.53 (28)
s(log_pop) + biome	26.5	27.72 (27)	0.85 (28)	0.35 (26)	0.55 (25)
biome + s(log_hs_density)	26.75	25.85 (25)	0.86 (26)	0.37 (24)	0.5 (32)
biome + region	30.5	45.9 (34)	0.84 (30)	0.32 (29)	0.51 (29)
region + s(ΣFRPnight)	30.75	34.45 (31)	0.83 (31)	0.28 (31)	0.5 (30)
s(log_pop) + region	31.75	42.62 (32)	0.82 (32)	0.26 (32)	0.5 (31)
s(log_pop) + s(log_hs_density)	32.5	33.65 (30)	0.81 (34)	0.25 (33)	0.48 (33)
region + s(log_hs_night_density)	33.5	44.11 (33)	0.81 (33)	0.23 (34)	0.48 (34)
region + s(ΣFRP)	35	46.95 (35)	0.79 (35)	0.22 (35)	0.44 (35)
region + s(log_hs_density)	36	57.97 (36)	0.76 (36)	0.19 (36)	0.39 (36)